International Journal of Hydrological and Environmental for Sustainability
Volume 5, Issue 3, 225-246.
e_ISSN: 2828-5050
https://www.journal.foundae.com/index.php/ijhes

Integrated HVSR Microtremor and Electrical Resistivity Analysis for Identifying Shallow Fluid Migration Pathways in Sangubanyu, Central Java, Indonesia

Hartono*
Departement of Physics,
Universitas Islam Negeri Walisongo Semarang,
INDONESIA

Oscar Kaeni
CV. Ardhipta Shona Persada Semarang,
INDONESIA

Jasuri
Departement of Physics,
Universitas Islam Negeri Walisongo Semarang,
INDONESIA

***Correspondence: E-mail:** hartono@walisongo.ac.id

Article Info

Article history:

Received: March 11, 2026
Revised: June 18, 2026
Accepted: July 30, 2026

Copyright : © 2026 Foundae (Foundation of Advanced Education). Submitted for possible open access publication under the terms and conditions of the Creative Commons Attribution - ShareAlike 4.0 International License (CC BY SA) license (https://creativecommons.org/licenses/by-sa/4.0/).

Abstract

Surface manifestations of oil seepage and geothermal discharge indicate active subsurface fluid migration, but identifying shallow migration pathways in structurally complex volcanic terrains remains challenging using a single geophysical method. This study investigates shallow fluid migration in the Sangubanyi area, Central Java, Indonesia, through the integrated interpretation of Horizontal-to-Vertical Spectral Ratio (HVSR) microtremor measurements and Schlumberger resistivity sounding. HVSR-derived shear-wave velocity (Vs) models were integrated with resistivity-depth models to constrain subsurface layering and identify geophysical boundaries related to fluid migration. MSB-02 exhibits a dominant frequency of 1.32 Hz with an amplification factor of 4.32. The representative Vs model consists of a low-velocity layer of approximately 380 m/s extending to a depth of about 70 m, underlain by a higher-velocity layer of approximately 1900 m/s. Resistivity models reveal conductive zones of approximately 7–30 Ω·m contrasting with resistive volcanic units exceeding 500 Ω·m. The coincidence between the Vs impedance contrast and the resistivity anomaly is interpreted as a geophysical boundary associated with lithological variation and fault-related deformation. Integrated interpretation suggests that fault- and fracture-related permeability provides the principal vertical pathway for fluid ascent, whereas the more permeable Kaligetas Formation facilitates lateral fluid redistribution, explaining the close spatial association between hot spring manifestations and localized oil seepage. Based on the available near-surface geophysical evidence, the seepage is interpreted as a localized surface expression of structurally controlled shallow fluid migration rather than direct evidence of significant shallow hydrocarbon accumulation.

Keywords: HVSR, electrical resistivity, shear-wave velocity, fluid migration, oil seepage, geothermal manifestation

To cite this article: Hartono., Kaeni, O. and Jasuri. (2026). Integrated HVSR Microtremor and Electrical Resistivity Analysis for Identifying Shallow Fluid Migration Pathways in Sangubanyu, Central Java, Indonesia. *International Journal of Hydrological and Environmental for Sustainability, 5*(3), 225-246. https://doi.org/10.58524/ijhes.v5i3.1175

INTRODUCTION

Surface manifestations such as oil seeps and geothermal fluid discharges represent critical indicators of active subsurface fluid circulation in regions characterized by complex tectonic and volcanic settings. Hydrocarbon seepage at the surface reflects the vertical migration of fluids from deeper petroleum systems through structurally controlled permeable pathways (Hosseini et al., 2022; Leifer, 2019). In many volcanic and sedimentary environments, subsurface fluid migration is strongly governed by geological structures including faults, fractures, lithological discontinuities, and permeable volcanic units that control subsurface permeability and fluid connectivity (Sibson, 1996;

Caine et al., 1996; Faulds & Hinz, 2015). Fault-related fracture systems commonly serve as preferential pathways for hydrothermal fluids, groundwater circulation, and hydrocarbon seepage, particularly in areas influenced by volcanic activity and tectonic deformation (Mazzini & Etiope, 2017; Curewitz & Karson, 1997). Variations in rock mechanical properties, porosity, alteration intensity, and fluid saturation associated with structurally controlled zones can generate geophysical contrasts detectable in both seismic and electrical rock properties (Revil et al., 2011; Telford et al., 1990). Accordingly, understanding the relationship between shallow subsurface heterogeneity, structural discontinuities, and fluid manifestations is fundamental for interpreting potential fluid circulation pathways in complex volcanic environments.

The Sangubanyu area, located in Batang Regency, Central Java, Indonesia, lies within the North Serayu Zone, which is characterized by Quaternary volcanic activity, tectonic deformation, and structurally controlled geomorphology. The regional geology of the area is dominated by volcanic deposits associated with the Central Java volcanic complex and fault systems that contribute to subsurface heterogeneity and permeability distribution (Condon et al., 1996; van Bemmelen, 1949). Based on the Geological Map of the Banjarnegara–Pekalongan Sheet (Condon et al., 1996), the study area is primarily underlain by the Kaligetas Formation (Q_{pkg}) and the Jembangan Volcanic Rocks (Q_j). The Kaligetas Formation consists of volcanic breccia, lava, tuffaceous sandstone, tuff, and claystone, whereas the Jembangan Volcanic Rocks comprise andesitic lava, volcanic breccia, pyroclastic deposits, and lahar. Both volcanic units have undergone varying degrees of fracturing, weathering, and hydrothermal alteration, producing secondary porosity and permeability that facilitate shallow fluid circulation and the development of fluid-related geophysical anomalies. Structural lineaments with a dominant northwest–southeast orientation have been identified within the regional geological framework and are interpreted to control the distribution of permeable zones and surface manifestations in the Sangubanyu area (Sudiono et al., 2019). These geological conditions suggest that the interaction between volcanic lithology, structural discontinuities, and shallow hydrogeological processes plays a significant role in controlling near-surface fluid manifestations in the study area.

The surface manifestations identified in the Sangubanyu area include oil seeps and geothermal fluid discharges occurring within a volcanically and structurally constrained environment. The spatial association between these two manifestation types suggests that shallow structural discontinuities, such as fractures and fault-related permeable zones, may influence fluid migration toward the surface. Nevertheless, the concurrent presence of hydrocarbon seepage and geothermal manifestations does not necessarily imply a single, hydraulically connected subsurface fluid system. Instead, the two manifestation types may originate from distinct fluid systems that share structurally controlled migration pathways within fractured volcanic rocks and permeable shallow formations (Mazzini & Etiope, 2017; Faulds & Hinz, 2015). In Indonesia, geothermal exploration has demonstrated that surface manifestations serve as critical proxies for identifying subsurface exploration targets, particularly in volcanic settings where structural controls on fluid flow are pervasive (Hochstein & Sudarman, 2008). In structurally complex volcanic environments, fault zones and fracture networks generally enhance secondary permeability and facilitate both vertical and lateral fluid circulation, ultimately producing localized fluid manifestations at the surface (Sibson, 1996; Curewitz & Karson, 1997). Therefore, characterizing shallow subsurface heterogeneity and structure-controlled permeable zones is essential for evaluating the potential relationship between geological structures and near-surface fluid manifestations in the Sangubanyu area.

Geophysical methods provide effective non-invasive approaches for investigating shallow subsurface heterogeneity associated with structure-controlled fluid zones in volcanic environments. The Horizontal-to-Vertical Spectral Ratio (HVSR) microtremor technique is widely employed to identify shallow impedance contrasts, resonance characteristics, and subsurface discontinuities through the analysis of ambient seismic noise (Nakamura, 1989; Bard, 1999; Molnar et al., 2022). HVSR data processing is commonly performed using the Geopsy software package, which offers a comprehensive and open-source environment for ambient vibration analysis (Wathelet et al., 2020). Shear-wave velocity (V_s) models derived from HVSR inversion are particularly useful for characterizing low-velocity zones associated with fractured, weathered, or mechanically weakened volcanic materials that may indicate enhanced permeability (Molnar et al., 2022; Trichandi et al., 2024). However, HVSR inversion is inherently non-unique, meaning that multiple subsurface models

may reproduce similar HVSR responses (Wathelet et al., 2004). In structurally complex volcanic environments, this ambiguity can hinder the interpretation of shallow structures and their relationship to fluid manifestations. In contrast, electrical resistivity methods in particular Vertical Electrical Sounding (VES) are highly sensitive to variations in fluid saturation, porosity, conductive clay alteration, and subsurface permeability distribution (Revil et al., 2011; Everett, 2013). The VES method with Schlumberger array configuration enables the derivation of 1D resistivity models that reflect vertical variations in rock properties and has been extensively applied in volcanic and hydrothermal environments (Perdomo et al., 2021; Ouchene et al., 2022). Low-resistivity anomalies in volcanic and hydrothermal settings are commonly associated with fluid-bearing structures, altered volcanic materials, or conductive permeable zones that may influence shallow fluid circulation (Umar et al., 2021; Yanis et al., 2022). Because HVSR and electrical resistivity respond to distinct yet complementary physical properties, the integration of mechanical impedance contrasts and electrical anomalies can provide a more physically constrained interpretation of shallow subsurface heterogeneity. Although geophysical methods cannot directly confirm active fluid migration, integrated analysis of mechanical and electrical contrasts can provide important constraints for identifying structure-controlled zones potentially associated with shallow fluid circulation and subsurface fluid pathways.

Previous geophysical investigations in the Sangubanyu area and analogous volcanic environments have generally applied microtremor or electrical resistivity methods independently, leaving the relationship between shallow mechanical contrasts, conductive anomalies, and structure-controlled fluid zones poorly constrained (Sudjono et al., 2019; Umar et al., 2021). HVSR-based studies have proven effective in identifying resonance characteristics and potential shallow discontinuities; however, the interpretation of representative subsurface models remains challenging due to the non-uniqueness inherent in HVSR inversion (Wathelet et al., 2004; Tawakal et al., 2020). On the other hand, resistivity methods can identify conductive anomalies potentially associated with fluid-bearing structures or altered volcanic materials, yet resistivity data alone cannot uniquely distinguish between lithological contrasts, alteration zones, and fluid-saturated permeable pathways (Revil et al., 2011; Everett, 2013; Ebong et al., 2022). As a result, single-method geophysical interpretations are susceptible to ambiguity in complex volcanic settings, particularly where shallow heterogeneity, alteration, and fracture systems develop concurrently.

To address these limitations, the present study implements an integrated interpretation framework that combines HVSR-derived mechanical contrasts with independently obtained resistivity depth information to improve the characterization of structure-controlled shallow zones. In this approach, the correspondence between major impedance contrasts and significant resistivity anomalies at comparable depths serves as the primary basis for constraining the selection of representative Vs models and interpreting structure-related shallow fluid pathways. This integration framework yields a more physically constrained interpretation of shallow subsurface heterogeneity while simultaneously reducing the ambiguity associated with HVSR inversion in structurally complex volcanic environments.

Building on this integrated framework, the present study aims to investigate shallow subsurface heterogeneity and structure-controlled fluid zones in the Sangubanyu area, Central Java, Indonesia, through the joint analysis of HVSR microtremor data and Vertical Electrical Sounding (VES). Specifically, this study focuses on: (1) identifying shallow impedance contrasts and deriving representative shear-wave velocity (Vs) models from HVSR inversion; (2) characterizing shallow resistivity variations associated with conductive and permeable subsurface zones; and (3) integrating mechanical and electrical anomalies at comparable depths to interpret structure-controlled shallow zones potentially associated with fluid circulation pathways. Through the integration of independently acquired geophysical parameters, this study aims to provide a more physically constrained interpretation of shallow subsurface conditions in a structurally complex volcanic environment.

METHOD

Study Area and Research Workflow

This study was conducted in Sangubanyu Village, Bawang District, Batang Regency, Central Java, Indonesia. The study area is characterized by the presence of a geothermal manifestation (G-01) and oil seepages (OS-01 and OS-02) developed within a volcanic environment. The spatial distribution of HVSR microtremor measurement points, Vertical Electrical Sounding (VES) stations, surface manifestations, geological units, and interpreted faults is illustrated in **Figure 1**. The study area is traversed by an interpreted fault that is presumed to influence subsurface heterogeneity and the spatial distribution of surface manifestations. Field data acquisition was conducted in December 2025. A total of two HVSR microtremor measurement points, designated MSB-01 and MSB-02, and five VES stations, designated GSB-03, GSB-04, GSB-05, GSB-06, and GSB-08, were employed in this study. Measurement locations were selected based on the distribution of surface manifestations, the position of the interpreted fault, field accessibility, and the requirement for spatial integration between HVSR and resistivity datasets.

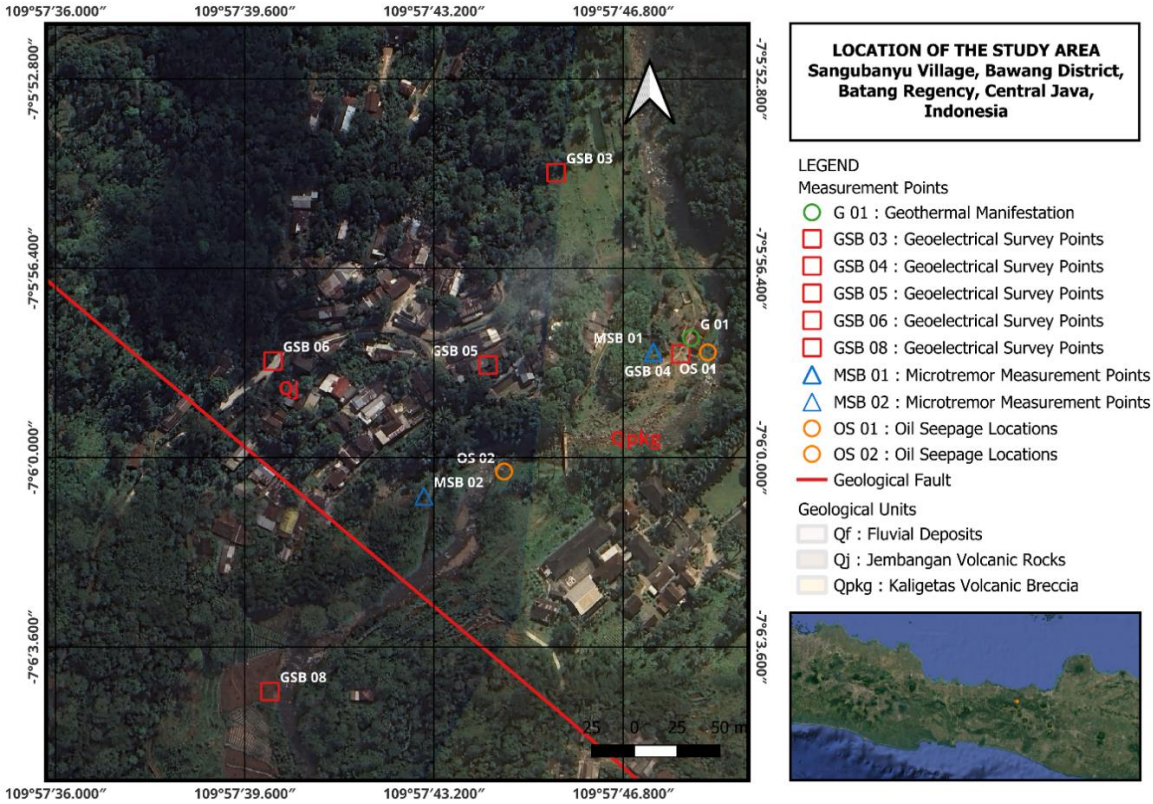

Figure 1. Location of the Sangubanyu study area, Central Java, Indonesia, and the spatial distribution of observation points

Stations MSB-01 and GSB-04 were positioned within the vicinity of geothermal manifestation G-01 and oil seepage OS-01. Station MSB-01 is located 24 m from G01 and 32 m from OS01, whereas VES point GSB-04 is situated 11 m from G01 and 15 m from OS01. This configuration was designed to characterize the subsurface conditions at a locality exhibiting the concurrent presence of geothermal manifestations and oil seepages. Station MSB-02 was established adjacent to geoelectrical sounding point GSB-05 and close to oil seepage OS-02 to facilitate the integration of HVSR-derived shear-wave velocity (*Vs*) models with resistivity sounding results at a common investigation point. The station was strategically positioned to characterize the mechanical properties of the shallow subsurface in the vicinity of the oil seepage and to provide complementary information for evaluating the relationship between lithological variations, subsurface physical properties, and shallow fluid migration.

The VES stations were arranged along two intersecting profiles that cross the interpreted fault zone. The first profile comprises stations GSB-03, GSB-05, and GSB-08, whereas the second profile

consists of stations GSB-04, GSB-05, and GSB-06. This measurement configuration was designed to obtain information on lateral resistivity variations within the fault-influenced zone and to provide resistivity constraints that can be compared with the shear wave velocity (*Vs*) models derived from HVSR inversion.

Figure 2 presents the research workflow employed in this study. The investigation commenced with a geological review and surface manifestation identification to determine optimal measurement locations. Subsequently, HVSR and VES data were acquired, subjected to quality control procedures, processed, and inverted to obtain shear wave velocity (*Vs*) models and subsurface resistivity models, respectively. Both models were then integrated with regional geological structure information and surface manifestation data to identify potential fluid migration pathways and to construct a subsurface geological model as the basis for final interpretation.

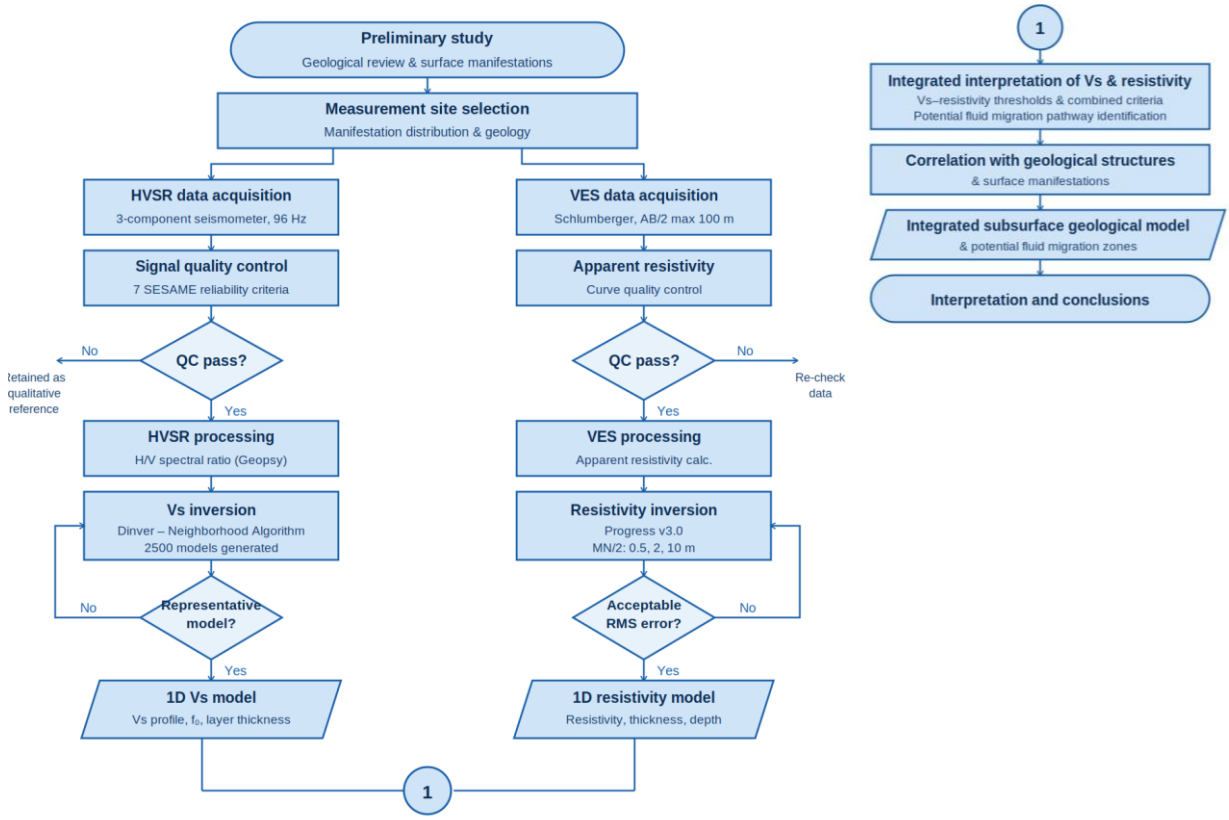

Figure 2. Research flowchart

HVSR Microtremor Data Acquisition and Processing

Microtremor measurements were conducted using a Sara Electronics VELBOX instrument (SL06 version) equipped with an SS02 three-component velocity sensor (E-W, N-S, and Z components) to record ambient ground vibrations at several locations distributed across the seepage and geothermal manifestation zones. Recordings were performed at a sampling frequency of 96 Hz, with a recording duration of approximately 60 minutes per measurement point. The sensor was installed in a three-component orthogonal orientation comprising the E-W, N-S, and vertical (Z) components. Ambient vibration methods such as HVSR are widely applied for site characterization and shallow subsurface investigation owing to their non-invasive nature and sensitivity to impedance contrasts (Molnar et al., 2022).

The recorded signals were processed using Geopsy software (version 4.8.7) to compute the Horizontal-to-Vertical Spectral Ratio (HVSR). The HVSR method is based on the ratio between horizontal and vertical spectral amplitudes, expressed as Equation (1).

$$\text{HVSR}\,(f) = \frac{H(f)}{V(f)} \qquad (1)$$

where $H(f)$ is the horizontal spectral amplitude and $V(f)$ is the vertical spectral amplitude at frequency f. The horizontal component is computed from two orthogonal components (NS and EW) as defined in Equation (2).

$$\mathrm{H}(f) = \sqrt{\frac{NS(f)^2 + EW(f)^2}{2}} \quad (2)$$

The processing workflow comprised: selection of stationary time windows; Fourier transformation for each component; computation of the H/V ratio; and spectral smoothing. A fixed time window length of 50 seconds with a 5% inter-window overlap was adopted in this study. Spectral smoothing was performed using the Konno-Ohmachi method with a smoothing constant of 40, over an analysis frequency range of 0.25–15 Hz. Windows containing transient noise were excluded based on a bad sample threshold of 99%.

The reliability of the dominant frequency is contingent upon the relationship between window length and frequency. In accordance with widely adopted HVSR reliability criteria, $f_0 > \frac{10}{l_w}$, where (l_w) denotes the time window length (SESAME, 2004). For this study, the minimum reliable frequency is fmin = 0.20 Hz. Reliability assessment of the HVSR curves was performed according to the SESAME (2004) criteria, encompassing seven aspects: (1) dominant frequency reliability ($f_0 > \frac{10}{l_w}$); (2) number of cycles ($N_c > 200$); (3) peak amplitude ($A_0 > 2$); (4) frequency stability ($\sigma_f < \varepsilon(f_0)$); (5) peak clarity; (6) well-defined peak width; and (7) amplitude variability and inter-window consistency. Fulfillment of all seven criteria is a prerequisite before an HVSR curve can proceed to the Vs inversion stage. This requirement is based on the consideration that curves failing to satisfy all criteria indicate spectral instability, poorly defined peaks, or significant noise contamination, which, if subjected to inversion, may yield unrepresentative Vs models and potentially erroneous interpretations. Curves that do not fulfill all SESAME criteria are not advanced to the inversion stage but are retained as qualitative reference data.

From a physical perspective, the dominant frequency (f_0) is interpreted as the fundamental resonance frequency, generally associated with the impedance contrast between soft surface layers and harder underlying material (Molnar et al., 2022). This frequency is related to the thickness and shear wave velocity of the sediment layer as defined in Equation (3).

$$[f_0 \approx \frac{V_s}{4H}] \quad (3)$$

where Vs is the shear wave velocity and H is the layer thickness. This relationship provides a first-order approximation for subsurface stratification (Molnar et al., 2022). Selected HVSR curves were inverted using the Dinver software module to obtain one-dimensional (1D) Vs models. The inversion employs a layered earth model and minimizes the misfit between the observed and calculated HVSR curves as defined in Equation (4).

$$[\varphi = \sum_{i=1}^{N} [HVSR_{obs}(f_i) - HVSR_{cal}(f_i)]^2] \quad (4)$$

As HVSR inversion is inherently non-unique, model selection is not based solely on the misfit value but also on geological plausibility and consistency with resistivity data (Piña-Flores et al., 2017).

HVSR Inversion

HVSR curves satisfying the SESAME (2004) quality and reliability criteria were subsequently inverted using the Dinver software module, which is part of the Geopsy software package. The inversion was performed to obtain a one-dimensional (1D) shear wave velocity (Vs) model of the subsurface capable of reproducing the observed HVSR curve. Dinver employs the Neighborhood Algorithm (NA) to explore the model parameter space and search for the parameter combination that yields the best fit between the observed and theoretical HVSR curves (Wathelet et al., 2008).

The subsurface model is represented as a layered model consisting of two layers above a half-space. The inverted parameters include compressional wave velocity (Vp), shear wave velocity (Vs), layer thickness, and Poisson's ratio, while density was held constant throughout the inversion to reduce the number of free parameters and improve solution stability. The inversion parameter

ranges were determined based on the geological characteristics of the study area, which is dominated by Quaternary volcanic rocks comprising andesite, andesitic breccia, weathered rock, and fracture zones developed around geothermal manifestations and oil seepages. The selected parameter ranges used in the Dinver inversion are summarized in **Table 1**.

Table 1. HVSR inversion parameters using Dinver

Parameter	Layer 1	Layer 2
Vp (m/s)	500–5000	3000–5500
Vs (m/s)	200–3500	1800–3500
Thickness (m)	5–100	Half-space
Poisson's ratio	0.05–0.50	0.20–0.50
Density (kg/m^3)	2000 (fixed)	2000 (fixed)

The parameter ranges presented in **Table 1** were adopted from commonly reported elastic property ranges for volcanic and shallow sedimentary materials (Telford et al., 1990; Kearey et al., 2002; Reynolds, 2011) and adjusted to reflect the expected subsurface conditions in the study area.The relatively wide Vs range was adopted to accommodate the possible presence of volcanic material with varying degrees of weathering, alteration, fracturing, and fluid saturation. A density value of 2000 kg/m^3 was used as a representative value for shallow volcanic material and was held constant during the inversion. The Vp and Poisson's ratio ranges were selected to represent the range of elastic conditions from relatively dry to fluid-saturated rock (Telford et al., 1990; Reynolds, 2011).

The inversion was performed using the Neighborhood Algorithm (NA) with search parameters of Itmax = 50, Ns0 = 50, Ns = 50, Nr = 50, and Nw = 2. These parameters were adopted to ensure adequate exploration of the model space while maintaining computational efficiency during the inversion process (Wathelet et al., 2008). The fit between the observed and theoretical HVSR curves was evaluated using the Equation (5).

$$\phi = \sum_{i=1}^{N}[HVSR_{obs}(f_i) - HVSR_{cal}(f_i)]^2 \qquad (5)$$

where ϕ is the misfit value; $HVSR_{obs}(f_i)$ is the observed HVSR value at frequency f_i; $HVSR_{cal}(f_i)$ is the theoretically calculated HVSR value at frequency f_i; and N is the number of frequency points used in the inversion process.

A lower value of ϕ indicates a better agreement between the theoretical model and the observed data. Models with the lowest misfit values that are still capable of reproducing the general shape of the observed HVSR curve are considered acceptable models and are employed in subsequent evaluation stages (Wathelet et al., 2008). As HVSR inversion is inherently a non-unique inverse problem, the model with the lowest misfit does not necessarily represent the most geologically realistic condition, and multiple models may yield equally satisfactory H/V responses relative to the observed data (Wathelet et al., 2008; Molnar et al., 2022). Consequently, representative model selection was performed through an integrative approach combining HVSR and resistivity inversion results.

Model selection was conducted in three steps. First, a set of acceptable models was identified—those capable of reproducing the general shape of the observed HVSR curve with relatively low misfit values compared to other models. Second, the depth of the primary impedance contrast was identified, as indicated by a significant change in Vs between layers in the inversion models. Third, the depth of this impedance contrast was compared with the depth of the primary resistivity change obtained from Vertical Electrical Sounding (VES) inversion to evaluate the correspondence between the two methods. The model demonstrating the best correspondence between Vs and resistivity contrasts was selected as the representative model for further interpretation.

This approach enables the selection of a Vs model that not only provides a good mathematical fit to the HVSR curve but also exhibits geophysical consistency with the subsurface resistivity model. Shear wave velocity (Vs) primarily reflects the mechanical properties of the rock, while electrical resistivity is more sensitive to fluid content, porosity, and degree of alteration. Consequently, the selected model not only reproduces the HVSR response satisfactorily but is also consistent with the subsurface electrical characteristics derived from geoelectrical surveys.

Electrical Resistivity Sounding Acquisition and Inversion

Electrical resistivity data were acquired using the Vertical Electrical Sounding (VES) method with a Schlumberger electrode configuration to characterize vertical variations in subsurface resistivity. The Schlumberger configuration was selected for its sensitivity to vertical resistivity changes and its widespread application in hydrogeological, geothermal, and shallow geological structure investigations (Telford et al., 1990; Reynolds, 2011). Data acquisition was performed using a Bawono-Resistivitymeter-12Geoinv2-N instrument with the Schlumberger configuration. The current electrode spacing (AB) was incrementally expanded to a maximum half-spacing (AB/2) of 100 m to increase the depth of investigation, while the potential electrode spacing (MN/2) was set at three values: 0.5 m, 2 m, and 10 m adjusted progressively with increasing current electrode spacing from AB/2 = 2 m to 100 m. MN spacing adjustments were implemented to maintain measurement sensitivity and to ensure an adequate AB/MN ratio at each measurement stage.

Apparent resistivity values were calculated using the relationship between the measured potential difference and the injected current, expressed as Equation (6).

$$\rho_a = K\frac{\Delta V}{I} \qquad (6)$$

where ρ_a is the apparent resistivity (Ωm); K is the geometric factor of the Schlumberger configuration; ΔV is the measured potential difference (V); and I is the injected current (A). The geometric factor for the Schlumberger configuration is calculated using the following equation (7)

$$K = \frac{\pi\left[\left(\frac{AB}{2}\right)^2 - \left(\frac{MN}{2}\right)^2\right]}{MN} \qquad (7)$$

where AB is the current electrode spacing and MN is the potential electrode spacing. Prior to inversion, the apparent resistivity data were subjected to a quality control procedure comprising evaluation of sounding curve continuity, identification of outliers, and assessment of possible effects from poor electrode contact, cultural noise, and measurement errors. Data exhibiting significant anomalous deviations were re-evaluated before being included in the inversion process.

The apparent resistivity data were subsequently inverted using Progress v3.0 software to obtain a one-dimensional (1D) subsurface resistivity model. The inversion was performed iteratively by minimizing the discrepancy between the observed apparent resistivity data and the theoretical model response using the following equation (8)

$$\varphi_p = \sum_{i=1}^{N}\left[\log \rho_{a,obs}(x_i) - \log \rho_{a,cal}(x_i)\right]^2 (8)$$

where φ_p is the resistivity inversion misfit value; $\rho_{a,obs}(x_i)$ is the observed apparent resistivity at measurement point x_i; $\rho_{a,cal}(x_i)$ is the calculated model apparent resistivity; and N is the number of observation data used in the inversion process. A lower value of φ_p indicates a better agreement between the theoretical model and the observed data.

As resistivity inversion is inherently a non-unique inverse problem, several different subsurface models may produce similar apparent resistivity responses (equivalence problem) (Orellana and Mooney, 1966; Zohdy et al., 1974). Consequently, interpretation of the resistivity model was not based solely on the mathematical fit of the inversion results but also considered the geological conditions of the study area and the shear wave velocity (V_s) inversion results obtained from HVSR analysis. This integrative approach was employed to reduce interpretive ambiguity and to improve the reliability of the subsurface model. The resistivity inversion results were subsequently used to identify lithological variations, alteration zones, fracture zones, and possible subsurface fluid migration pathways.

Integrated Interpretation of Vs and Resistivity

Final subsurface interpretation was conducted through the integration of the one-dimensional shear-wave velocity (1D Vs) model obtained from HVSR inversion and the one-dimensional resistivity (1D resistivity) model derived from Vertical Electrical Sounding (VES) inversion. The integration of these two independent geophysical methods was intended to reduce interpretative ambiguity and improve the reliability of the conceptual subsurface model. Each method provides complementary information regarding subsurface conditions. The Vs model primarily reflects the

mechanical characteristics of subsurface materials, whereas the resistivity model is more sensitive to their electrical properties. Consequently, the combined interpretation provides a more comprehensive understanding of lithological variations, weathering conditions, fracture development, and possible fluid-bearing zones than either method alone (Telford et al., 1990; Reynolds, 2011).

Shear-wave velocity (*Vs*) mainly represents the elastic and mechanical properties of rocks, including rock stiffness, degree of compaction, weathering intensity, and fracture development. In contrast, electrical resistivity is strongly influenced by porosity, fluid saturation, alteration intensity, clay content, and the electrical conductivity of subsurface materials. Because these two parameters respond to different physical properties, they are considered complementary for geological interpretation, particularly in volcanic terrains where lithological heterogeneity and structural complexity often produce non-unique interpretations when a single geophysical method is employed (Telford et al., 1990; Reynolds, 2011; Milson & Eriksen, 2011).

To provide a consistent basis for integrating both parameters, general interpretation criteria were established using parameter ranges commonly reported in geophysical literature and subsequently adapted to the geological characteristics of the study area. These criteria summarize the typical ranges of shear-wave velocity and electrical resistivity together with their corresponding geophysical significance and general geological interpretation. The integrated interpretation criteria adopted in this study are presented in **Table 2**. The interpretation criteria presented in **Table 2** served as the initial reference for integrating the Vs and resistivity models. It should be emphasized that these criteria represent general guidelines rather than absolute classification boundaries because the physical properties of rocks may vary depending on lithology, weathering degree, alteration processes, and local geological conditions. Therefore, the parameter ranges were used to support geological interpretation instead of serving as the sole basis for lithological identification.

The integration procedure was performed in several stages. First, the Vs inversion model and the resistivity inversion model were analyzed independently to identify major changes in shear-wave velocity and electrical resistivity with depth. These changes were interpreted as potential boundaries between subsurface layers exhibiting contrasting physical properties. Subsequently, the depth correspondence between the major contrasts identified in both models was evaluated. Where significant changes in Vs and resistivity occurred at comparable depths, these boundaries were interpreted as representing the same geological interface, thereby increasing confidence in the interpreted subsurface stratigraphy.

Table 2. Integrated Vs–resistivity interpretation criteria

Parameter	Range	Geophysical Significance	General Interpretation*
Low Vs	< 500 m/s	Low rock stiffness, low shear modulus	Potentially associated with weathered material, loose sediments, or fractured zones.
Moderate Vs	500–1000 m/s	Moderate rock stiffness	Potentially associated with moderately weathered or fractured volcanic rocks.
High Vs	> 1000 m/s	High rock stiffness, high impedance contrast	Potentially associated with relatively compact volcanic rocks or basement.
Low resistivity	< 30 Ωm	High electrical conductivity	Potentially associated with alteration zones, fluid saturation, or fine-grained material (e.g., clay).
Moderate resistivity	30–100 Ωm	Moderate conductivity	Potentially associated with weathered rock, partially fluid-filled fractures, or moderate alteration.
High resistivity	> 100 Ωm	Low conductivity (resistive)	Potentially associated with relatively compact rock, low alteration, and relatively low fluid content.

Following the identification of corresponding layer boundaries, each subsurface layer was interpreted using the combined characteristics of Vs and resistivity rather than relying on either parameter individually. The preliminary interpretation derived from **Table 2** was subsequently refined by considering the consistency between both geophysical models and incorporating regional

geological information, mapped geological structures, and field observations collected during the survey. This multi-parameter approach reduces the uncertainty associated with the non-unique nature of individual geophysical methods and provides a more robust basis for geological interpretation.

One of the principal objectives of this integrated interpretation was to identify subsurface zones that may facilitate fluid migration. In this study, the term potential fluid migration pathway refers to subsurface zones where the combined geophysical characteristics indicate enhanced permeability, commonly associated with fractured, weathered, or altered rocks. The designation of such zones was based on the spatial correspondence between relatively low to moderate Vs, low to moderate resistivity, geological structural evidence, and the occurrence of surface oil seepages. Therefore, the identified pathways should be regarded as indicators of potentially favorable conditions for fluid migration rather than direct evidence of active fluid flow or hydrocarbon accumulation.

Finally, the geological interpretation was completed through a comprehensive evaluation integrating the Vs model, resistivity model, regional geological framework, interpreted geological structures, and the distribution of observed surface manifestations. The final conceptual subsurface model was established only after all available evidence demonstrated mutual consistency. This integrative approach minimizes interpretative uncertainty and provides a more reliable representation of subsurface geological conditions than interpretations derived from individual geophysical methods alone.

RESULTS AND DISCUSSION

HVSR Analysis Results

The Horizontal-to-Vertical Spectral Ratio (HVSR) curves derived from microtremor measurements at stations MSB-01 and MSB-02 are presented in **Figure 3**. Each curve represents the average H/V spectrum computed from multiple selected time windows, while the colored lines illustrate the response of individual windows employed to evaluate the stability of the resonance frequency. The HVSR curves were subsequently assessed against the SESAME (2004) reliability criteria to determine their suitability as input for Vs inversion.

At station MSB-01 (**Figure 3a**), the HVSR curve exhibits a relatively broad peak within the frequency range of approximately 2–3 Hz, with a dominant frequency of $f_0 = 3.00 \pm 0.50$ Hz and an amplification factor of $A_0 = 2.19$. The broad resonance peak and the relatively large inter-window variability indicate that the subsurface impedance contrast at this location does not develop strongly at a single layer boundary. Such characteristics are generally associated with a heterogeneous subsurface, weathered layers, or the presence of multiple overlapping impedance contrasts.

In contrast, the HVSR curve at station MSB-02 (**Figure 3b**) displays a single, sharp, and well-defined resonance peak at a dominant frequency of $f_0 = 1.32 \pm 0.07$ Hz, with an amplification factor of $A_0 = 4.32$. The narrow peak and consistent inter-window response indicate the presence of a stronger and more stable subsurface impedance contrast compared to MSB-01. These characteristics suggest a clearer layer boundary and satisfy the reliability criteria recommended by SESAME (2004).

Based on the evaluation in **Table 3**, both HVSR curves satisfy the criteria for reliable dominant frequency, sufficient number of cycles, and peak amplitude greater than two ($A_0 > 2$). However, only the HVSR curve at MSB-02 fulfills all SESAME reliability criteria, as evidenced by a well-defined sharp resonance peak, high dominant frequency stability, and consistent inter-window amplitude. Conversely, the HVSR curve at MSB-01 exhibits a broad resonance peak with greater frequency variability, satisfying only a portion of the reliability criteria. Consequently, only the HVSR curve at MSB-02 was selected for shear wave velocity (Vs) inversion because it satisfied all SESAME reliability criteria, whereas the MSB-01 curve was retained solely as qualitative reference data.

The contrasting HVSR characteristics between MSB-01 and MSB-02 indicate lateral variations in the dynamic subsurface response within the study area. These variations were further analyzed through Vs inversion and compared with resistivity inversion results to obtain a more comprehensive subsurface interpretation.

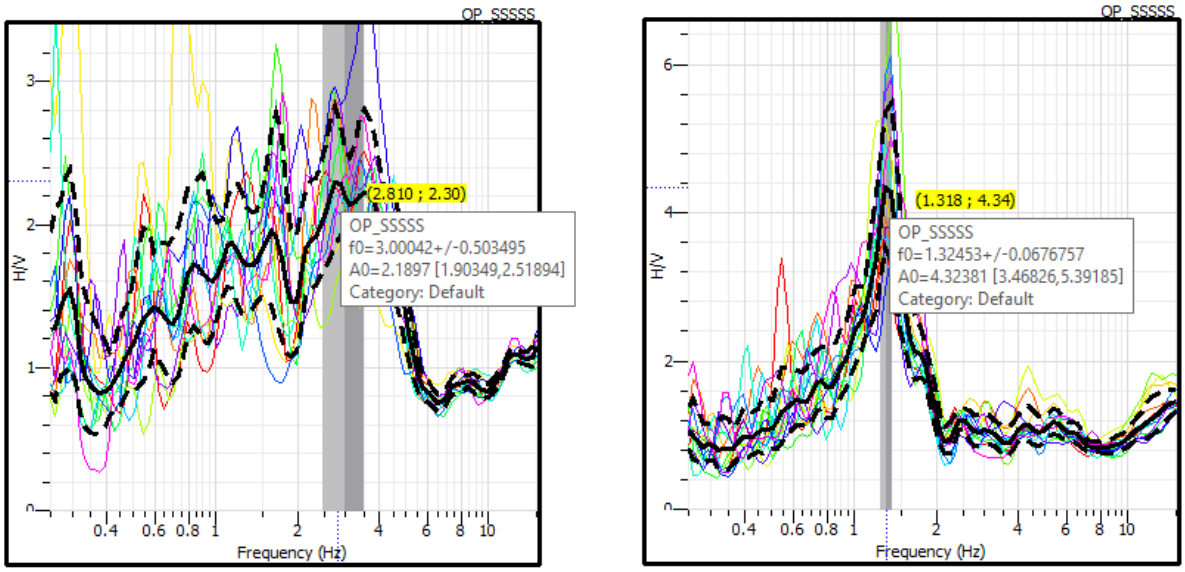

(a) (b)

Figure 3. HVSR curves derived from microtremor measurements at two observation points in the Sangubanyu area: (a) MSB-01 and (b) MSB-02. Colored lines represent individual time-window HVSR curves, the solid black line indicates the average HVSR curve, and the dashed black lines delineate the variability around the mean response

Table 3. HVSR curve reliability evaluation based on SESAME (2004) criteria

SESAME Criterion	MSB-01	MSB-02
Reliable dominant frequency	✓	✓
Sufficient number of cycles	✓	✓
Peak amplitude ($A_0 > 2$)	✓	✓
Inter-window frequency stability	X	✓
Peak clarity (well-defined peak)	X	✓
Appropriate peak width	X	✓
Inter-window amplitude stability	X	✓
Used for Vs inversion	**No**	**Yes**

Shear-Wave Velocity (Vs) Inversion Results

Based on the HVSR curve reliability evaluation, only the HVSR curve from station MSB-02 satisfied all SESAME (2004) reliability criteria and was therefore selected for deriving the subsurface shear-wave velocity (Vs) model. The inversion was performed using the Dinver module within the Geopsy software package, employing the Neighborhood Algorithm, yielding a set of models capable of reproducing the observed HVSR curve within the defined misfit threshold. As HVSR inversion is inherently a non-unique inverse problem, multiple subsurface models may produce equally adequate HVSR responses. Accordingly, the model selected for interpretation is not exclusively the one with the lowest misfit value, but the model deemed most representative based on its fit to the observed curve, geological consistency, and consistency with the resistivity inversion results obtained in this study.

The inversion models at station MSB-02 exhibit a relatively consistent pattern (**Figure 4**). The majority of models indicate the presence of a low shear wave velocity layer in the shallow portion, with Vs values of approximately 350–450 m/s extending to depths of approximately 60–80 m. Below this layer, a pronounced increase in Vs to approximately 1800–3000 m/s is observed, indicating a significant mechanical impedance contrast at those depths. This contrast is consistent with the sharp resonance peak and stable dominant frequency observed in the MSB-02 HVSR curve.

Although multiple models satisfy the defined misfit threshold, not all models possess the same degree of representativeness. Consequently, one model was selected as the representative Vs model for subsequent geological interpretation. Model selection was based on three primary criteria: (1) a satisfactory fit to the observed HVSR curve; (2) a consistent primary impedance contrast in the Vs

model; and (3) a good depth correspondence with the major resistivity changes derived from Vertical Electrical Sounding (VES) inversion. This approach was adopted to reduce the interpretive ambiguity commonly encountered in HVSR inversion and to improve the reliability of the subsurface model used in the integration stage. The parameters of the representative Vs model selected for interpretation are summarized in **Table 4**.

Table 4 demonstrates that all inversion models satisfying the misfit threshold share a common general characteristic: a shallow layer with low Vs values (203.63–464.93 m/s) overlain by a layer with significantly higher Vs values (1805.41–2777.55 m/s). Although the depth of the Vs contrast varies between 36.58 and 86.94 m across models, this general pattern emerges consistently throughout the full set of acceptable models. Inter-model depth variability reflects the nature of the non-unique inverse problem, wherein multiple subsurface configurations can produce equally satisfactory HVSR responses relative to the observed data. Therefore, at this stage, the inversion results are used to characterize the general subsurface structure, whereas the selection of the final representative model is based on its consistency with the independently derived resistivity model and the available geological information.

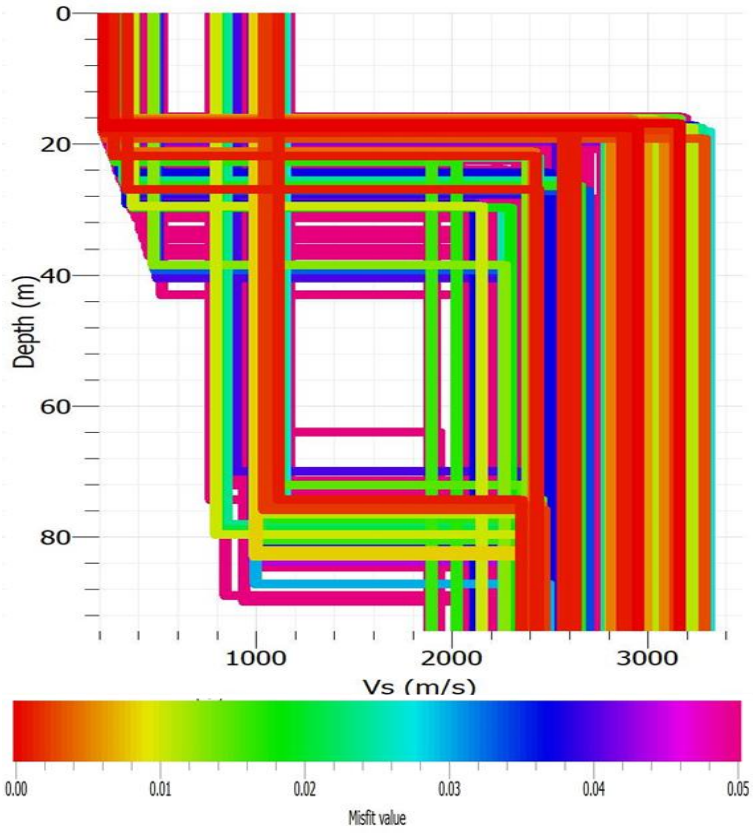

Figure 4. HVSR inversion results using the Dinver module at station MSB-02.

Table 4. Summary of HVSR inversion model parameters satisfying the misfit threshold at station MSB-02

Parameter	Inversion Results (38 acceptable models)	Notes
Number of acceptable models	38 models	All models satisfy the defined misfit threshold.
Vs of shallow layer	203.63–464.93 m/s	All models indicate a low-Vs surface layer.
Depth of Vs contrast	36.58–86.94 m	Depth variability reflects the non-unique nature of HVSR inversion.
Vs of deeper layer	1805.41–2777.55 m/s	All models show a significant Vs increase below the shallow layer.

The representative Vs model is subsequently employed as the basis for integration with the one-dimensional resistivity inversion results to evaluate the relationship between changes in rock mechanical properties and changes in subsurface electrical properties. The integration of both methods aims to reduce the interpretive ambiguity that may persist when each method is analyzed independently.

Geoelectrical Sounding Results

Apparent resistivity curves derived from Vertical Electrical Sounding (VES) measurements at five observation stations are presented in Figure 5. The curves illustrate the variation in apparent resistivity as a function of current electrode half-spacing (AB/2), reflecting changes in subsurface electrical properties at various depths of investigation. Based on Figure 5, station GSB-03 exhibits apparent resistivity values ranging from 11 to 52 Ωm, with relatively smooth variations as electrode spacing increases. The relatively low to moderate resistivity values indicate the presence of more conductive material at shallow to intermediate depths.

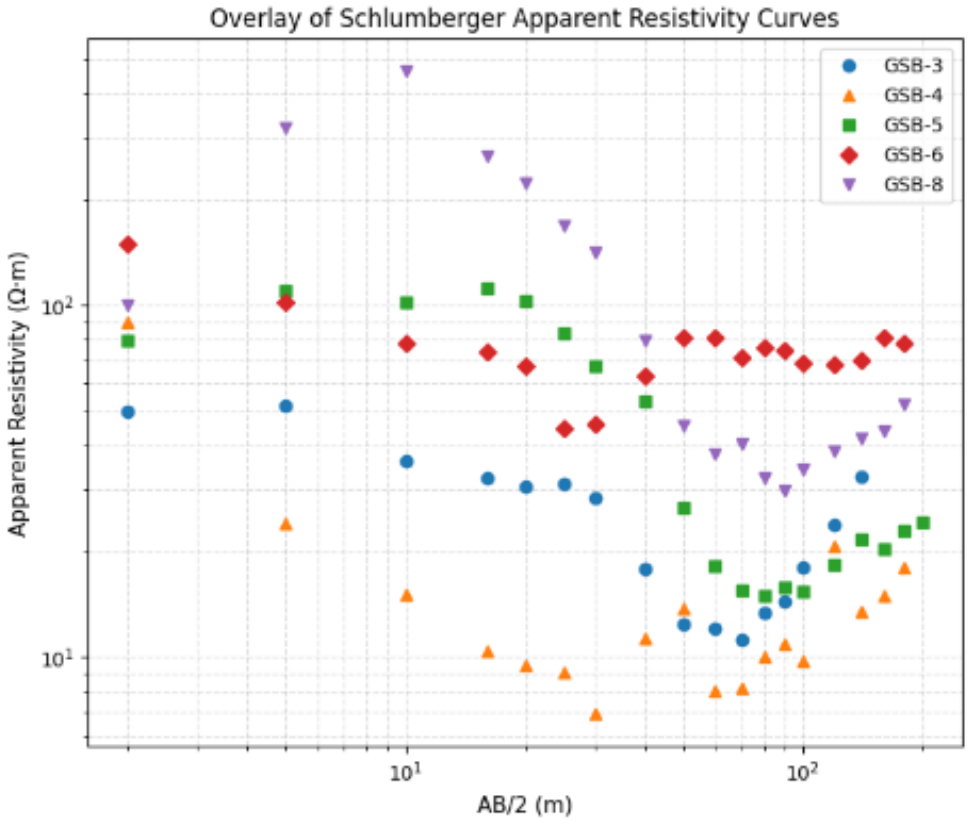

Figure 5. Apparent resistivity curves showing distinct variations among the VES stations, indicating lateral heterogeneity in subsurface electrical properties and suggesting differences in lithology, fluid saturation, or alteration intensity across the study area

Station GSB-04 shows an apparent resistivity range of approximately 7–90 Ωm, with a decreasing trend at intermediate electrode spacings. This characteristic indicates the presence of a more conductive subsurface layer compared to the other stations. At station GSB-5, apparent resistivity values increase to approximately 110 Ωm at small to intermediate spacings, subsequently decreasing to approximately 15–25 Ωm at larger spacings. This pattern indicates a vertical transition from a relatively resistive shallow layer toward a more conductive layer at greater depths. Station GSB-6 is characterized by relatively high and stable apparent resistivity values, ranging from approximately 45 to 150 Ωm, indicating the dominance of moderate to high resistivity material throughout most of the investigation depth.

Station GSB-08 exhibits the highest apparent resistivity values, reaching more than 500 Ωm at small electrode spacings, which subsequently decrease and converge toward 30–50 Ωm at larger spacings. This pattern indicates a strong resistivity contrast between the shallow and deeper layers.

Overall, all apparent resistivity curves display considerable variability at small electrode spacings (low AB/2), whereas at larger spacings the curves tend to converge. This pattern indicates that electrical heterogeneity is more pronounced in the shallow layers, while deeper layers exhibit relatively more uniform electrical characteristics. Based on the range of resistivity values obtained, the electrical response can generally be classified into three zones: low resistivity (<20 Ωm), moderate resistivity (20–100 Ωm), and high resistivity (>100 Ωm). This classification serves as the basis for interpreting the resistivity inversion results in the following subsection.

Table 5. Resistivity interpretation criteria used as reference for inversion result interpretation

Resistivity Range	Geophysical Interpretation	Possible Geological Significance
< 20 Ωm	Conductive zone	Altered material, fine-grained material (e.g., clay), or fluid-saturated zone.
20–100 Ωm	Moderate resistivity zone	Weathered, fractured, or moderately altered volcanic material; potentially fluid-bearing.
> 100 Ωm	Resistive zone	Relatively compact volcanic material with low alteration and minimal fluid content.

The resistivity ranges presented in **Table 5** are adopted as general guidelines for interpreting the resistivity inversion results in this study. The classification was formulated based on the resistivity characteristics obtained from field data and is referenced to the literature on volcanic rock interpretation (Telford et al., 1990; Reynolds, 2011). Accordingly, this classification is not absolute but serves as an initial framework for identifying possible lithology, degree of alteration, and potentially fluid-bearing zones prior to correlation with regional geological information.

The variability in apparent resistivity curves at the five sounding stations reflects heterogeneity in the subsurface electrical response in the vicinity of the geothermal manifestations and oil seepages. However, as the apparent resistivity curve represents a composite response of the entire subsurface column, identification of the vertical resistivity distribution requires one-dimensional (1D) inversion. Consequently, the apparent resistivity data were subjected to inversion to obtain true resistivity models, which subsequently serve as the basis for constructing geoelectrical cross-sections and geological interpretations in the following subsection.

One-dimensional resistivity models derived from Vertical Electrical Sounding (VES) inversion at the five sounding stations are presented in **Figure 6**. Each model illustrates the variation in resistivity with depth obtained through the inversion of apparent resistivity data. To facilitate interpretation, resistivity values are grouped into three classes: low resistivity (<20 Ωm), moderate resistivity (20–100 Ωm), and high resistivity (>100 Ωm). These classes were adopted as general interpretation guidelines for evaluating variations in subsurface electrical properties prior to the integrated interpretation with the shear-wave velocity (Vs) model.

The inversion models indicate that each sounding station exhibits distinct resistivity distribution characteristics, reflecting subsurface heterogeneity at the study locations. In general, all models display an alternation of layers with low, moderate, and high resistivity; however, the number of layers, their thicknesses, and depths vary among sounding stations. These variations demonstrate that subsurface conditions are not homogeneous, either vertically or laterally.

Among all sounding stations, GSB-05 exhibits the most pronounced resistivity contrasts, characterized by transitions between several high, moderate, and low resistivity layers from shallow to intermediate depths. In contrast, models at GSB-03 and GSB-06 show more gradual resistivity changes, while GSB-04 and GSB-08 display a relatively more complex alternation of conductive and resistive layers. These differing patterns indicate that subsurface electrical property changes do not develop uniformly throughout the study area.

The presence of low-resistivity layers generally indicates more conductive material, while high-resistivity layers reflect relatively more resistive material. Based on the interpretation classification in Section 4.5, these variations may be associated with changes in lithology, degree of alteration, fluid content, or the development of fracture zones. Nevertheless, resistivity is a non-unique parameter, meaning that a single resistivity value may represent more than one geological condition. Geological interpretation is therefore not conducted solely on the basis of resistivity models but requires integration with additional geophysical parameters.

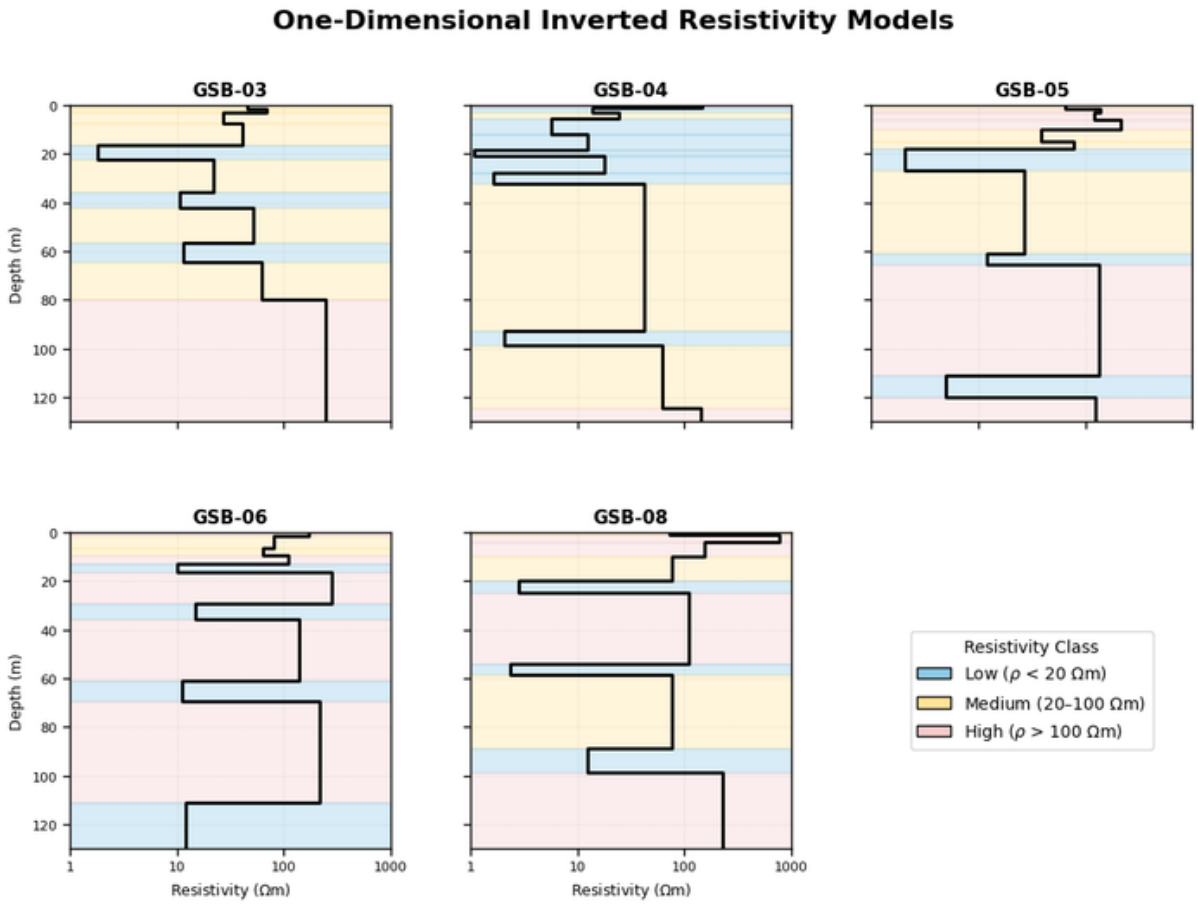

Figure 6. One-dimensional inverted resistivity models derived from Vertical Electrical Sounding (VES) at stations GSB-03, GSB-04, GSB-05, GSB-06, and GSB-08

Overall, the resistivity inversion results reveal heterogeneity in subsurface electrical properties developing both vertically and laterally at the study location. These resistivity models subsequently serve as the basis for integrated interpretation through comparison with the shear wave velocity (Vs) models derived from HVSR inversion. This integrative approach aims to reduce interpretive ambiguity and improve reliability in identifying subsurface characteristic changes potentially associated with geological structures and fluid migration.

Integrated Vs–Resistivity Results (1D Overlay)

Figure 7 presents the one-dimensional integration between the shear wave velocity (Vs) model derived from HVSR inversion at station MSB-02 and the resistivity model obtained from VES inversion at the nearest station. The Vs model was derived from HVSR curve inversion using the Dinver module, while the resistivity model was obtained independently from geoelectrical sounding data. Both models are plotted against a common depth axis to evaluate the correspondence between changes in mechanical and electrical subsurface properties.

The representative Vs model exhibits a shallow layer with Vs values of approximately 380 m/s extending to a depth of approximately 70 m. Below this depth, Vs increases significantly to approximately 1900 m/s, indicating a strong mechanical impedance contrast. This velocity contrast is interpreted as the boundary between a relatively weathered or fractured rock layer and a more compact rock layer at greater depths.

Comparison with the resistivity model reveals that this Vs change corresponds with a significant resistivity change at approximately the same depth. At a depth of approximately 70 m, resistivity transitions from approximately 18.6 Ωm to 245 Ωm. The spatial correspondence between the Vs contrast and the resistivity contrast provides stronger evidence for the existence of a real subsurface layer boundary compared to interpretations based on a single geophysical method. Although the resistivity model exhibits some shallow resistivity variations, most of these changes are

not associated with significant Vs variations. Conversely, the most pronounced correspondence between the two methods occurs at a depth of approximately 70 m, where both the Vs model and the resistivity model exhibit sharp transitions. This indicates that this layer boundary constitutes the primary geological feature controlling both the mechanical and electrical subsurface responses at the study location.

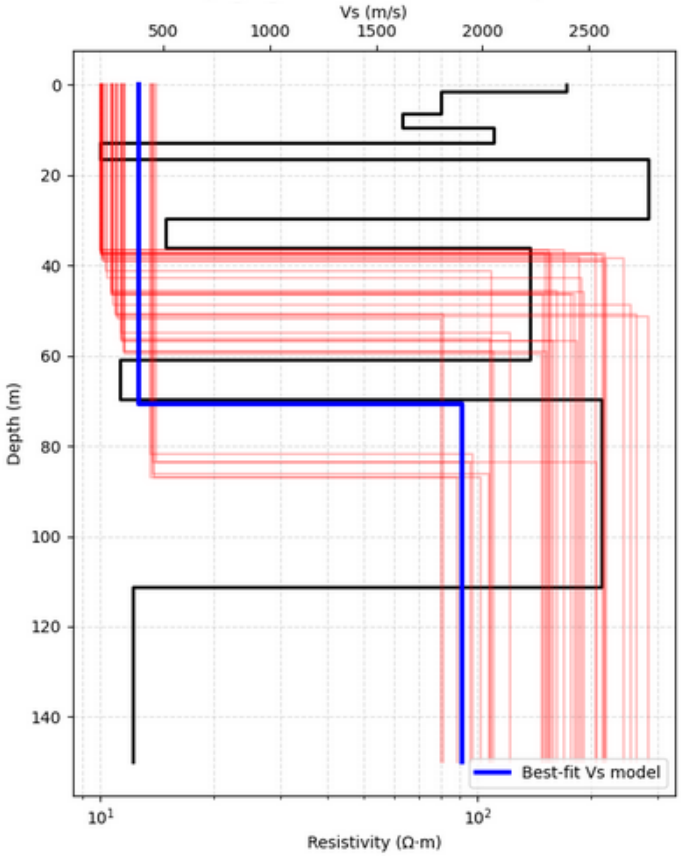

Figure 7. The 1D overlay between the HVSR-derived Vs models and the corresponding resistivity profile at MSB-02 shows that the selected best-fit Vs model is consistent with major resistivity contrasts, suggesting that the interpreted subsurface layering reasonably represents mechanically and electrically distinct zones potentially related to shallow fluid migration

It should be noted that HVSR inversion is non-unique, and the selected Vs model represents the most plausible model among a set of acceptable solutions. Nevertheless, the strong correspondence between the Vs contrast and the resistivity contrast provides independent support for the existence of the interpreted layer boundary, thereby increasing confidence in the derived subsurface model. Overall, the integration results demonstrate that changes in mechanical and electrical subsurface properties occur at approximately the same depth. This correspondence indicates the presence of an important geological transition zone and forms the basis for identifying potential fluid migration pathways in the subsequent integrated interpretation stage.

Discussion: Structural Control and Fluid Migration

The integrated interpretation based on geological data, resistivity inversion results, HVSR inversion models, and the integration of both geophysical methods indicates that the occurrence of hot spring manifestations and oil seepages in the Sangubanyu area is not governed by a single controlling factor, but rather represents the outcome of interactions among geological structures, lithological contrasts, and variations in subsurface rock physical properties. To elucidate these relationships, two geological cross-sections were interpreted: profile A–A' (GSB03–GSB05–GSB08) and profile B–B' (GSB06–GSB05–GSB04), integrating surface geological information with resistivity inversion results and the Vs model at GSB05 as the control point.

Profile A–A' (**Figure 8**) illustrates the lateral variation in subsurface conditions from the northern to the southern portion of the study area. Based on the geological map, this profile traverses

the boundary between the Kaligetas Formation (Qpkg) and the Jembangan Volcanic Rocks (Qj), thereby providing insight into changes in rock physical properties attributable to lithological differences.

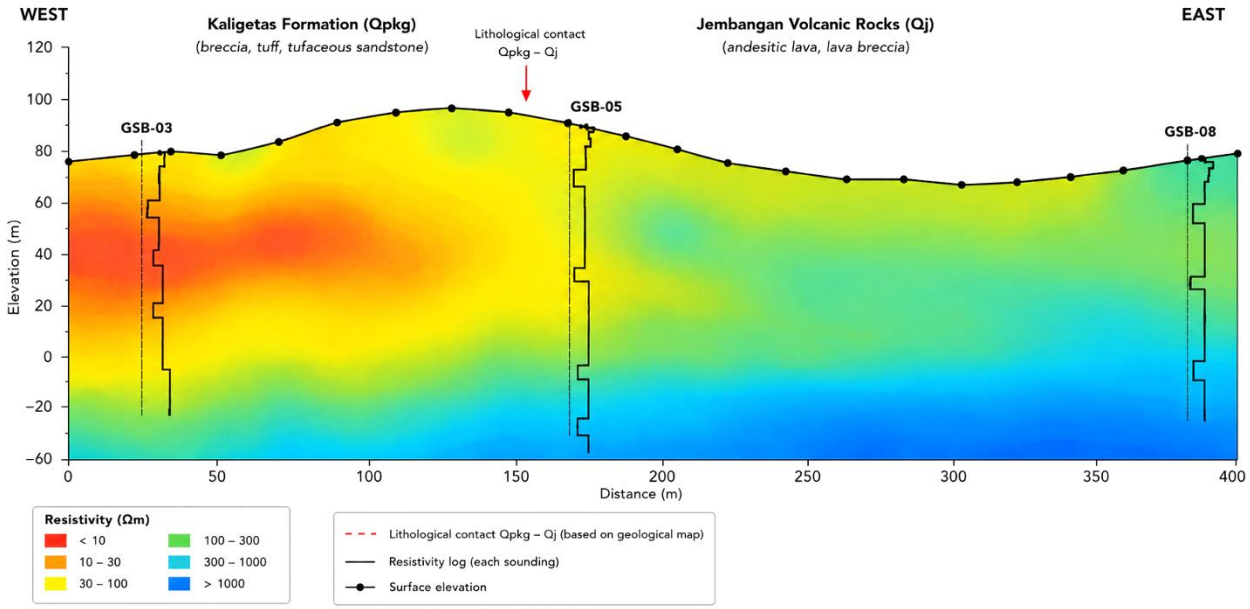

Figure 8. Interpreted geological cross-section along profile A–A' (GSB03–GSB05–GSB08) integrating topography, resistivity sounding results, and regional geological information

The interpretation results indicate that the portion corresponding to the Kaligetas Formation is dominated by low to moderate resistivity layers, interpreted as volcanic breccia, tuff, and tuffaceous sandstone that have undergone weathering and alteration. Conversely, the portion developed within the Jembangan Volcanic Rocks exhibits increasing resistivity, indicative of the presence of andesitic lava and flow breccia of greater compactness. This characteristic change is consistent with the lithological description in the regional geological map, which states that the Kaligetas Formation is composed of pyroclastic material that is relatively more permeable than the lava rocks comprising the Jembangan Formation.

Integration of the HVSR inversion model at station GSB-05 reveals a change in rock mechanical properties at a depth of approximately 70 m. The shallow layer is characterized by Vs values of approximately 380 m/s associated with low to moderate resistivity, while below this depth Vs increases significantly to approximately 1900 m/s, concurrent with an increase in rock resistivity. The correspondence between these two parameter changes indicates a strong contrast in both mechanical and electrical properties. This zone is interpreted as a geophysical boundary separating the relatively weathered, fractured, and more permeable shallow layer from the more compact volcanic rock at depth.

It must be emphasized that this geophysical boundary is not directly interpreted as a fault plane or lithological contact, but rather as a transition zone of rock physical properties spatially positioned in the vicinity of the contact between the two formations. Consequently, the Vs and resistivity changes at a depth of approximately 70 m are interpreted as a composite response resulting from lithological variation combined with the influence of geological structures developed within the study area. Profile B–B' (**Figure 9**) constitutes the primary cross-section connecting GSB06–GSB05–GSB04, intersecting the geothermal manifestation area and oil seepages. Compared to profile A–A', this cross-section provides clearer information on the relationship between geological structures and the distribution of subsurface fluids.

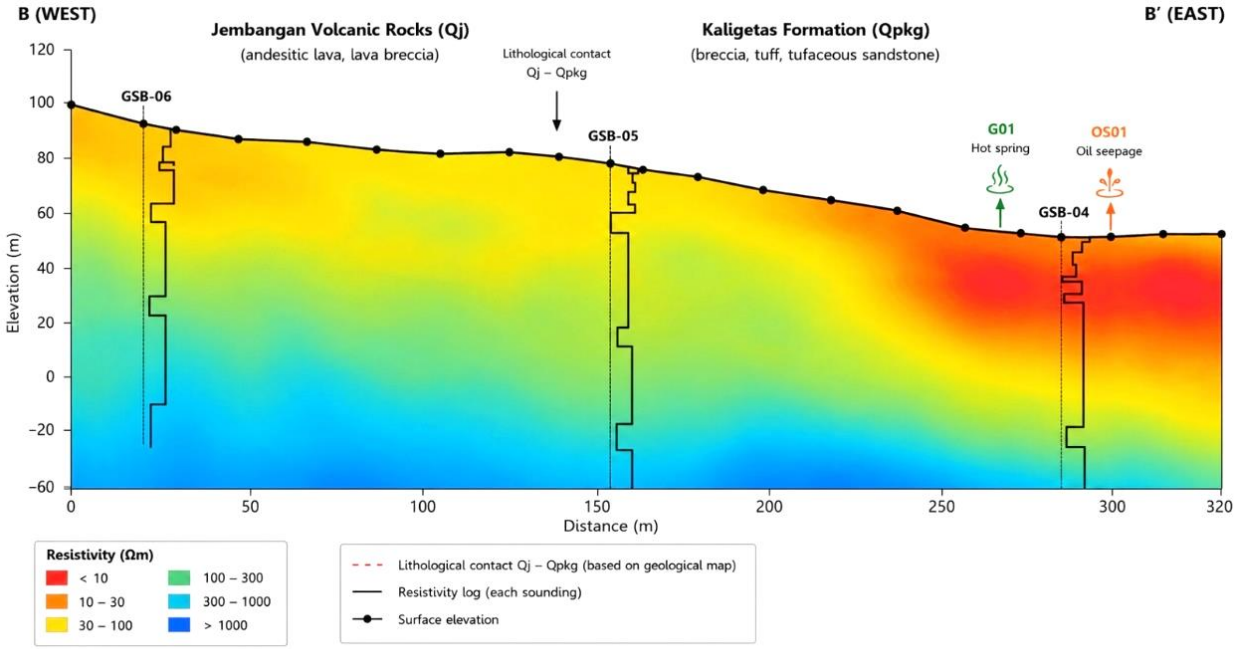

Figure 9. Interpreted geological cross-section along profile B–B' (GSB06–GSB05–GSB04) integrating topography, resistivity sounding results, and regional geological information

In the western portion of the profile, GSB-06, situated within the Jembangan Volcanic Rocks, is dominated by moderate to high resistivity. These values are interpreted as andesitic lava and flow breccia that remain relatively compact, possess low porosity, and have not undergone intensive hydrothermal alteration. A similar condition is observed at GSB-08, indicating that resistive character represents a natural property of the Qj lithology. In contrast, GSB-04, situated within the Kaligetas Formation, exhibits predominantly low to moderate resistivity throughout almost the entire depth profile. These resistivity values are interpreted as pyroclastic rock that has undergone weathering and hydrothermal alteration, accompanied by the development of fractures that increase fluid content within the rock. Notably, this location is also directly associated with the hot spring manifestation (G-01) and oil seepage (OS-01), suggesting that the conductive zone reflects not only lithological influence but also the effects of alteration and fluid circulation processes.

Station GSB-05, positioned between the two aforementioned stations, exhibits transitional characteristics. Integration of the resistivity inversion results and the Vs model reveals a change in rock physical properties at a depth of approximately 70 m, dividing the rock into two principal zones: a relatively soft, fractured, and more permeable shallow layer and a more compact underlying layer. The position of GSB05 in proximity to the lithological contact and adjacent to geological structures renders this station the most representative location for integrating the two geophysical methods. The interpretation of both cross-sections indicates that the geologically mapped fault likely functions as the primary conduit for fluid migration from depth toward the surface. However, the distribution of surface manifestations demonstrates that fluids do not emerge directly above the fault trace, but are displaced toward the Kaligetas Formation, which possesses more permeable physical properties.

This interpretation is supported by the geoelectrical results and Vs model, which indicate that the Kaligetas Formation exhibits lower resistivity and smaller Vs values compared to the Jembangan Volcanic Rocks. These conditions suggest the development of more weathered, altered, and higher-permeability rock that is more readily traversed by fluids compared to the relatively compact andesitic lava. Accordingly, the fault is interpreted as functioning as a vertical fluid migration pathway from depth, while the Kaligetas Formation acts as a medium for lateral fluid dispersal at shallow depths. The combination of these two mechanisms results in the emergence of hot spring manifestations and oil seepages at locations in close proximity to, but not directly above, the fault plane. It should be noted that the geophysical data employed in this study are insufficient to establish that the fault plane is precisely located at a depth of approximately 70 m. Therefore, the change in rock physical properties at this depth is more appropriately interpreted as a geophysical or

mechanical boundary associated with concurrent lithological variation and the influence of geological structures.

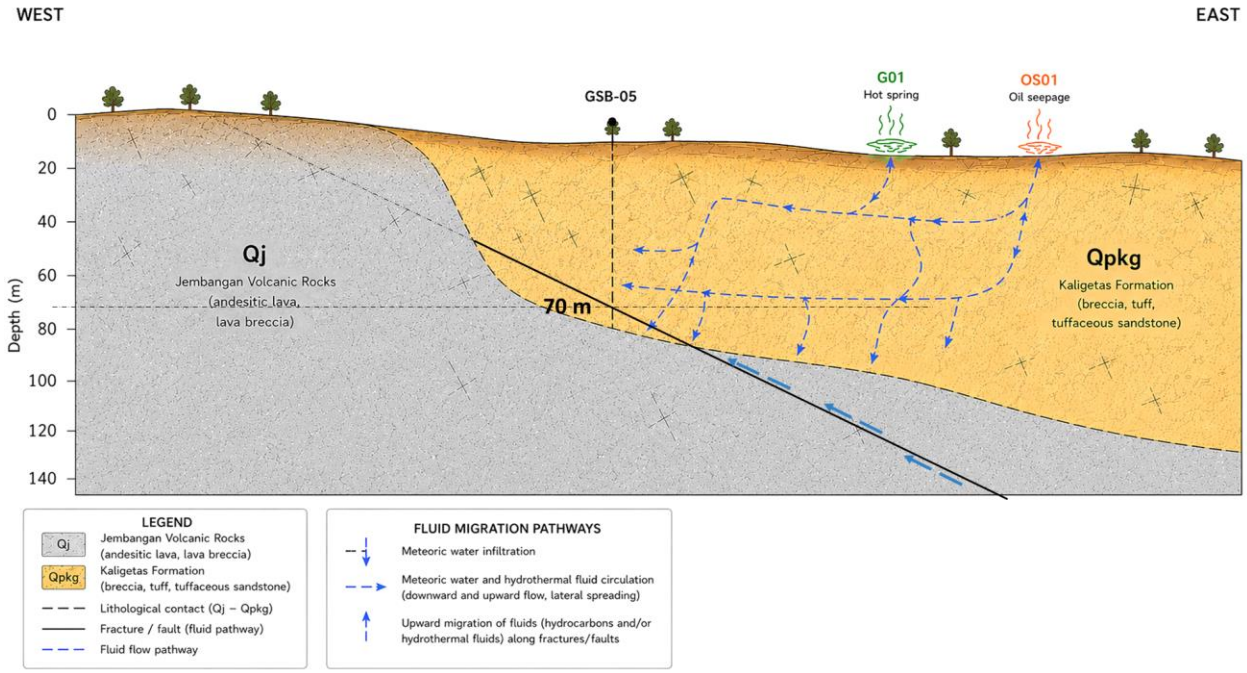

Figure 10. Proposed conceptual model of shallow fluid migration in the Sangubanyi area.

Based on all interpretation results, a conceptual model of fluid migration in the Sangubanyu area is presented in **Figure 10**. This model indicates that the hydrothermal and hydrocarbon systems likely originate from different sources but exploit the same migration pathways toward the surface. Meteoric water infiltrating through fractures is estimated to undergo heating at depth and subsequently migrate upward through the fault zone. Simultaneously, hydrocarbons originating from source rocks at greater depths also migrate through the same structural pathway. Upon reaching the shallow zone, both fluids enter the Kaligetas Formation, which possesses higher permeability, and undergo lateral dispersal through the fracture network and rock pore spaces before ultimately emerging as hot spring manifestations and oil seepages at the surface. This model explains why both manifestations occur at nearby locations without necessarily implying that they originate from the same reservoir. Consequently, the structural system in the study area is more appropriately interpreted as a shared migration pathway for both fluid types, while the hydrothermal and hydrocarbon fluid sources remain two distinct geological systems.

CONCLUSION

The integrated interpretation of Schlumberger resistivity sounding and HVSR microtremor data successfully characterized the shallow subsurface beneath the Sangubanyi manifestation area and demonstrated the value of combining both methods for evaluating structurally controlled fluid migration. The HVSR analysis identified the dominant resonance at MSB-02 and a representative shear-wave velocity model consisting of a low-velocity layer of approximately 380 m/s extending to a depth of about 70 m, underlain by a higher-velocity layer of approximately 1900 m/s, while the resistivity models revealed a coincident contrast from relatively conductive to more resistive volcanic rocks. This agreement between the Vs and resistivity contrasts is interpreted as a geophysical boundary associated with changes in lithology and fault-related deformation rather than a direct identification of either the fault plane or lithological contact. The integrated geological interpretation suggests that fault- and fracture-related permeability provides the principal vertical pathway for fluid ascent, whereas the relatively permeable Kaligetas Formation (Q_{pkg}) facilitates lateral fluid migration, explaining the close spatial association between the hot spring manifestation and localized oil seepage. Based on the available near-surface geophysical evidence, the observed

seepage is interpreted as a localized surface expression of structurally controlled shallow fluid migration rather than direct evidence of significant shallow hydrocarbon accumulation, indicating that the integration of HVSR-derived shear-wave velocity and resistivity models provides an effective framework for identifying shallow geophysical boundaries and evaluating fluid migration pathways in structurally complex volcanic terrains.

AUTHOR CONTRIBUTIONS

Conceptualization, H and OK; methodology, H and J; software, OK; validation, H and OK; formal analysis, J and OK; investigation, H; resources, H and J; data curation, H; writing—original draft preparation, OK; writing—review and editing, H and J; visualization, H; supervision, H and J; project administration.

ACKNOWLEDGMENT

The authors sincerely thank the reviewers for their valuable comments and constructive suggestions, which have significantly improved the quality and clarity of this manuscript.

CONFLICTS OF INTEREST

The authors declare no conflict of interest concerning the publication of this article. The authors also confirm that the data and the article are free of plagiarism.

REFERENCES

Bard, P.-Y. (1999). Microtremor measurements: A tool for site effect estimation? In K. Irikura, K. Kudo, H. Okada, & T. Sasatani (Eds.), The Effects of Surface Geology on Seismic Motion (pp. 1251–1279). Balkema.

Caine, J. S., Evans, J. P., & Forster, C. B. (1996). Fault zone architecture and permeability structure. Geology, 24(11), 1025–1028. https://doi.org/10.1130/0091-7613(1996)024<1025:FZAAPS>2.3.CO;2

Condon, W. H., Pardyanto, L., Ketner, K. B., Amin, T. C., Gafoer, S., & Samodra, H. (1996). Peta Geologi Lembar Banjarnegara dan Pekalongan, Jawa [Geological map of the Banjarnegara and Pekalongan Sheet, Java] (Scale 1:100,000). Pusat Penelitian dan Pengembangan Geologi.

Curewitz, D., & Karson, J. A. (1997). Structural settings of hydrothermal outflow: Fracture permeability maintained by fault propagation and interaction. Journal of Volcanology and Geothermal Research, 79(3–4), 149–168. https://doi.org/10.1016/S0377-0273(97)00027-9

Ebong, E. D., Akwueke, E. D., & Sunday, N. E. (2022). Combined application of vertical electrical sounding and 2D electrical resistivity tomography for groundwater exploration in parts of Enugu metropolis, southeastern Nigeria. International Journal of Physical Sciences, 17(3), 67–83. https://doi.org/10.5897/IJPS2021.4976

Everett, M. E. (2013). Near-Surface Applied Geophysics. Cambridge University Press. https://doi.org/10.1017/CBO9781139088435

Faulds, J. E., & Hinz, N. H. (2015). Favorable tectonic and structural settings of geothermal systems in the Great Basin region, western USA: Proxies for discovering blind geothermal systems. Proceedings World Geothermal Congress 2015, Melbourne, Australia.

Hochstein, M. P., & Sudarman, S. (2008). History of geothermal exploration in Indonesia from 1970 to 2000. Geothermics, 37(3), 220–266. https://doi.org/10.1016/j.geothermics.2008.01.001

Hosseini, A., Saberi, M. H., & ZareNezhad, B. (2022). Significance of petroleum seepages in hydrocarbon exploration: Case study of Khourian Desert, Central Iran. Journal of Petroleum Exploration and Production Technology, 12, 1649–1663. https://doi.org/10.1007/s13202-021-01440-7

Kearey, P., Brooks, M., & Hill, I. (2002). An Introduction to Geophysical Exploration (3rd ed.). Blackwell Science.

Leifer, I. (2019). A synthesis review of emissions and fates for the Coal Oil Point marine hydrocarbon seep field and California marine seepage. Geofluids, 2019, 4724587. https://doi.org/10.1155/2019/4724587

Mazzini, A., & Etiope, G. (2017). Mud volcanism: An updated review. Earth-Science Reviews, 168, 81–112. https://doi.org/10.1016/j.earscirev.2017.03.001

Milsom, J., & Eriksen, A. (2011). Field Geophysics (4th ed.). Wiley-Blackwell.

Molnar, S., Sirohey, A., Assaf, J., Bard, P.-Y., Castellaro, S., Cornou, C., Cox, B., Guillier, B., Hassani, B., Kawase, H., Matsushima, S., Clinton, J., D'Amico, S., Mayeda, K., Poggi, V., Psarropoulos, P., Sørensen, M. B., Spica, Z., & Zerva, A. (2022). A review of the microtremor horizontal-to-vertical spectral ratio (MHVSR) method. Journal of Seismology, 26(4), 653–685. https://doi.org/10.1007/s10950-021-10062-9

Nakamura, Y. (1989). A method for dynamic characteristics estimation of subsurface using microtremor on the ground surface. Quarterly Report of the Railway Technical Research Institute, 30(1), 25–33.

Orellana, E., & Mooney, H. M. (1966). Master Tables and Curves for Vertical Electrical Sounding over Layered Structures. Interciencia.

Ouchene, A., Bouyahiaoui, B., Abtout, A., Bourouis, S., & Gibert, D. (2022). Vertical electrical sounding (VES) technique to map potential aquifers of the Guigou Plain (Middle Atlas, Morocco): Hydrogeological implications. Applied Sciences, 12(24), 12829. https://doi.org/10.3390/app122412829

Perdomo, S., Ainchil, J. E., & Kruse, E. E. (2021). Vertical electrical sounding (VES) for estimation of hydraulic parameters in the porous aquifer. Water, 13(2), 170. https://doi.org/10.3390/w13020170

Piña-Flores, J., Perton, M., García-Jerez, A., Carmona, E., Luzón, F., Molina-Villegas, J. C., & Sánchez-Sesma, F. J. (2017). The inversion of spectral ratio H/V in a layered system using the diffuse field assumption (DFA). Geophysical Journal International, 208(1), 577–588. https://doi.org/10.1093/gji/ggw416

Revil, A., Finizola, A., Piscitelli, S., Rizzo, E., Ricci, T., Crespy, A., Angeletti, B., Morin, J., & Baudin, T. (2011). Hydrogeology of Stromboli volcano, Aeolian Islands (Italy) from the interpretation of resistivity tomograms, self-potential, soil temperature and soil CO2 concentration measurements. Geophysical Journal International, 186(3), 1078–1094. https://doi.org/10.1111/j.1365-246X.2011.05112.x

Reynolds, J. M. (2011). An Introduction to Applied and Environmental Geophysics (2nd ed.). Wiley-Blackwell.

SESAME. (2004). Guidelines for the implementation of the H/V spectral ratio technique on ambient vibrations: Measurements, processing and interpretation (SESAME European Research Project, WP12 – Deliverable D23.12). European Commission.

Sibson, R. H. (1996). Structural permeability of fluid-driven fault-fracture meshes. Journal of Structural Geology, 18(8), 1031–1042. https://doi.org/10.1016/0191-8141(96)00032-6

Sudjono, Purwanto, H. S., & Husein, S. (2019). Identifikasi struktur geologi bawah permukaan berdasarkan data mikrotremor di daerah Sangubanyu, Kabupaten Batang, Jawa Tengah [Identification of subsurface geological structures based on microtremor data

in the Sangubanyu area, Batang Regency, Central Java]. Prosiding Seminar Nasional Kebumian ke-12, Universitas Gadjah Mada, Yogyakarta, 5–6 September 2019.

Tawakal, M. I., Marliyani, G. I., & Nurdiyanto, B. (2020). Estimating shear wave velocity (Vs30) of East Java, Indonesia, using ambient noise inversion of horizontal to vertical spectral ratio (HVSR). IOP Conference Series: Earth and Environmental Science, 538, 012012. https://doi.org/10.1088/1755-1315/538/1/012012

Telford, W. M., Geldart, L. P., & Sheriff, R. E. (1990). Applied Geophysics (2nd ed.). Cambridge University Press. https://doi.org/10.1017/CBO9781139167932